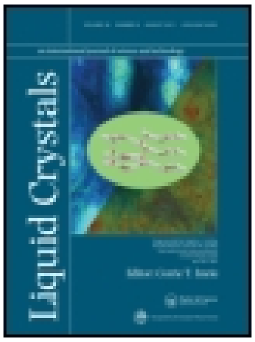

Liquid Crystals

ISSN: 0267-8292 (Print) 1366-5855 (Online) Journal homepage: https://www.tandfonline.com/loi/tlct20

Polar smectic phases in quasi-bent-core liquid crystals with hockey-stick-shaped mesogen: synthesis and crossover mesomorphism

E-Joon Choi, Hye-Jin Kim, Seung-Chang Kang, Dae-Yoon Kim, Kwang-Un Jeong, You-Jin Lee, Chang-Jae Yu & Jae-Hoon Kim

To cite this article: E-Joon Choi, Hye-Jin Kim, Seung-Chang Kang, Dae-Yoon Kim, Kwang-Un Jeong, You-Jin Lee, Chang-Jae Yu & Jae-Hoon Kim (2019): Polar smectic phases in quasi-bent-core liquid crystals with hockey-stick-shaped mesogen: synthesis and crossover mesomorphism, Liquid Crystals, DOI: 10.1080/02678292.2019.1630492

To link to this article: https://doi.org/10.1080/02678292.2019.1630492

LIQUID CRYSTALS
https://doi.org/10.1080/02678292.2019.1630492

Polar smectic phases in quasi-bent-core liquid crystals with hockey-stick-shaped mesogen: synthesis and crossover mesomorphism

E-Joon Choi[a], Hye-Jin Kim[a], Seung-Chang Kang[a], Dae-Yoon Kim[b], Kwang-Un Jeong[b], You-Jin Lee[c], Chang-Jae Yu[c] and Jae-Hoon Kim[c]

[a]Department of Polymer Science and Engineering, Kumoh National Institute of Technology, Gumi, Gyungbuk, Korea; [b]Department of Polymer-Nano Science and Technology, Chonbuk National University, Jeonju, Korea; [c]Department of Electronic Engineering, Hanyang University, Seoul, Korea

ABSTRACT

New hockey-stick-shaped liquid crystals (HSLCs) have been designed and synthesised. By extreme shortening of one 'arm' in the HSLCs, we have constructed the pronounced overall hockey-stick-shaped molecular conformation of these materials, and called the pseudo-rod-like (PRL) molecules with hockey-stick-shaped mesogen. The chemical structures were identified using spectroscopy and elemental analysis. The mesomorphic behaviour was investigated by polarising optical microscopy (POM), differential scanning calorimetry (DSC), X-ray diffractometry (XRD), and via electro-optical experiments. As a result, in spite of the PRL molecules, the various mesomorphic polymorphism, the interdigitated bi-layered structure and macroscopic polarity were found. Similar to up-to-date HSLCs, the quasi-bent-core LCs showed a transition from the synclinic SmC phase (SmC$_s$) to anticlinic SmC (SmC$_a$) phase, and exhibited SmA-type (N$_{CybA}$) and SmC-type (N$_{CybC}$) cybotactic nematic phases. At the same time, similar to practical rod-like LCs, the PRL molecules showed good surface alignment behaviour under planar boundary conditions.

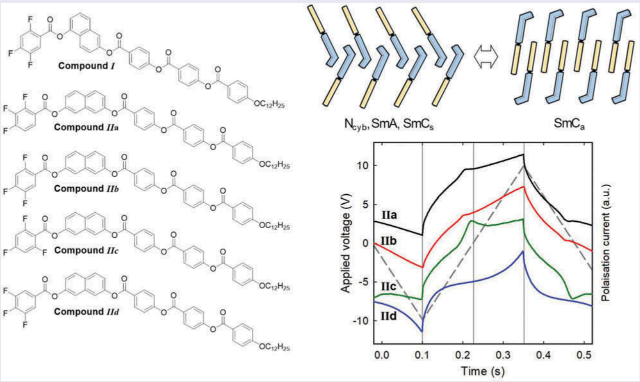

ARTICLE HISTORY
Received 30 April 2019
Accepted 6 June 2019

KEYWORDS
Polar symmetry; hockey-stick liquid crystals; mesophase polymorphism; interdigitated bilayer structure; uniform texture

1. Introduction

Over the recent two decades, there has been significant progress in liquid crystal science through understanding of mirror symmetry breaking and bulk polarity emergence [1]. The occurrence of chirality and spontaneous polarisation in achiral liquid crystals (LCs) have been of particular interest [2]. The recent findings include heliconical-tilted smectic (SmC$_{TB}$) phases in achiral dimesogenic compounds [3]. In addition, cutting-edge evolvement has been made towards macroscopic polarity, which stems from the potential polar symmetry as a result of the high structural variability of bent-core liquid crystals (BCLCs) [4,5]. The current state-of-the-art is hockey-stick-shaped liquid crystals (HSLCs), which were designed as intermediates between the linear rod-like liquid crystals (RLLCs) and non-linear BCLCs [6–34]. From a structural point of view, classification of HSLCs reported in the literature would provide the knowledge of structure–property relationship being useful for the design of targeted HSLCs for novel applications in relevant LC fields. In this regard, we recently advocated that the molecular geometry of HSLCs can be divided into three categories (see Scheme 1) [27,30]: (i) type 1:

CONTACT E-Joon Choi ejchoi@kumoh.ac.kr
Supplemental data for this article can be accessed here.

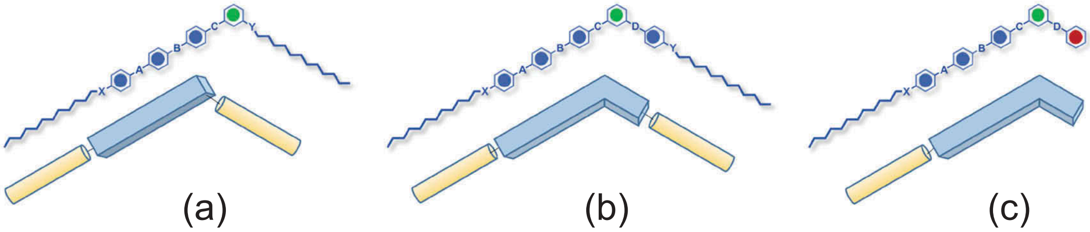

Scheme 1. (Colour online) Reported hockey-stick-shaped liquid crystals (HSLCs) by category (blue block = mesogenic unit; yellow block = flexible terminal). (a, b) Types 1 and 2 (HSLCs-**1** and **2**) have two long arms, which can participate in C_{2v} packing. (c) Type 3 (HSLCs-**3**) has one long arm and one that is too short to play a role in the polar packing.

asymmetric bent-shaped RLLCs (HSLCs-1) [6–9]; (ii) type 2: asymmetric BCLCs (HSLCs-2) [10–23]; (iii) type 3: pseudo-linear and quasi-bent-shaped HSLCs (HSLCs-3) [24–34]. HSLCs-1 and HSLCs-2 have flexible alkyl chains at each end of the mesogen, whereas HSLCs-3 possess a flexible alkyl chain on only one end of the mesogen. The first two types of molecules have atypical hockey-stick-shaped conformation, whereas the latter type has a pronounced hockey-stick-shaped conformation. Therefore, the HSLCs-3 can be much more efficient for the materialisation of intermediate mesogenic properties between those of BCLCs and RLLCs. For instance, recently achiral HSLCs have been demonstrated to form dark conglomerate (DC) phases [17], twist-bend phases [18], cluster phases [19,20], biaxial phases [31], and chiral random grain boundaries (RGBs) [32].

In this study, a new series of HSLCs-3 based on 1,6- or 2,7-naphthalene central core have been designed and synthesised (Scheme 2). The molecules possess trifluorophenyl groups on the short arms and tris-benzoyloxy units on the long arm, which has ester linkages with the same linking order. The structure was identified by using FT-IR and ^{1}H NMR spectroscopy and elemental analysis. The mesomorphic behaviour was investigated by using polarised optical microscopy (POM), differential scanning calorimetry (DSC), and X-ray diffraction (XRD). In the planar surface stabilised mesophases, the alignment behaviour was investigated by POM. The macroscopic polarity was also explored using a triangle-wave method.

2. Experimental

2.1. Synthesis

The synthetic route to compounds **I** and **IIa–d** is presented in Scheme 3. The synthetic procedures were based on a modification of the methods described in the literature [27]. The synthetic procedures and

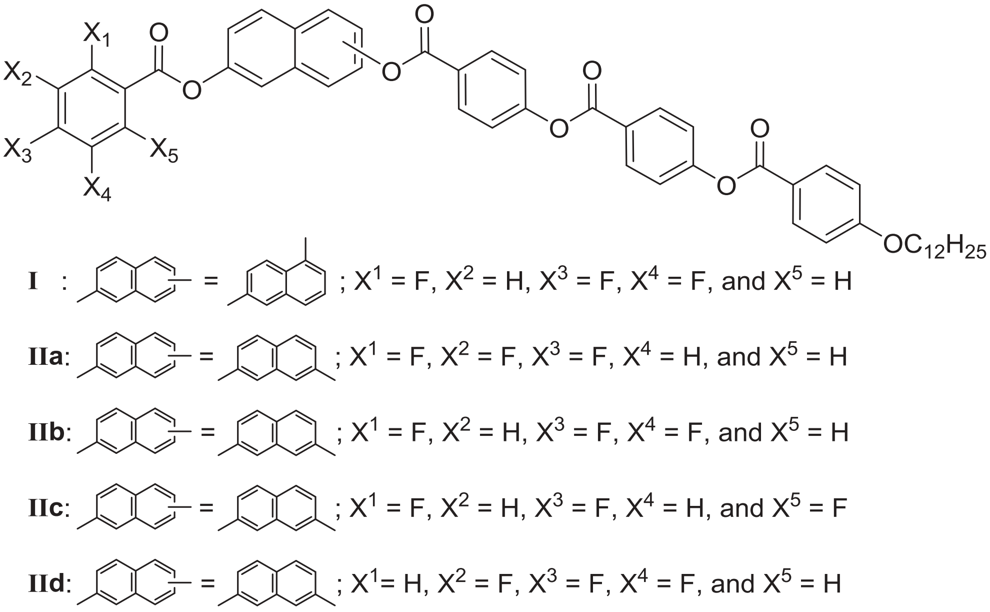

I : ; X^1 = F, X^2 = H, X^3 = F, X^4 = F, and X^5 = H

IIa: ; X^1 = F, X^2 = F, X^3 = F, X^4 = H, and X^5 = H

IIb: ; X^1 = F, X^2 = H, X^3 = F, X^4 = F, and X^5 = H

IIc: ; X^1 = F, X^2 = H, X^3 = F, X^4 = H, and X^5 = F

IId: ; X^1= H, X^2 = F, X^3 = F, X^4 = F, and X^5 = H

Scheme 2. Chemical structures of the HSLCs-**3** under investigation.

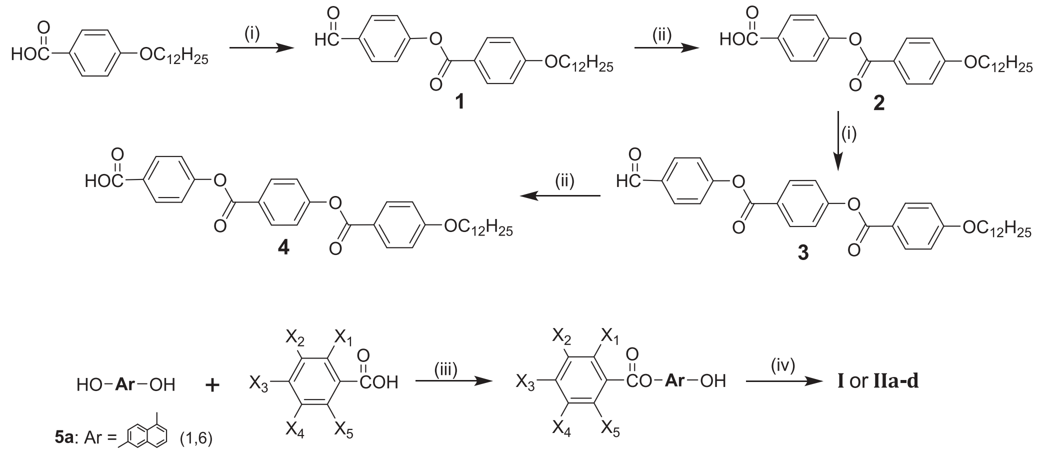

6 : Ar = 1,6; X^1 = F, X^2 = H, X^3 = F, X^4 = F, and X^5 = H
7a: Ar = 2,7; X^1 = F, X^2 = F, X^3 = F, X^4 = H, and X^5 = H
7b: Ar = 2,7; X^1 = F, X^2 = H, X^3 = F, X^4 = F, and X^5 = H
7c: Ar = 2,7; X^1 = F, X^2 = H, X^3 = F, X^4 = H, and X^5 = F
7d: Ar = 2,7; X^1= H, X^2 = F, X^3 = F, X^4 = F, and X^5 = H

Scheme 3. Synthetic route to compounds **I** and **IIa–d**: (i) 4-hydroxybenzaldehyde, DCC, DMAP, CH_2Cl_2; (ii) resorcinol, $NaClO_2$, NaH_2PO_4, THF; (iii) DCC, DMAP, CH_2Cl_2, CH_3CN; (iv) compound **4**, DCC, DMAP, CH_2Cl_2.

analytical data for the final compounds **I** and **IIa–d** are described below. The chemical structures were confirmed with IR and NMR spectra recorded using a Scinco Nicolet 6700 FTIR and a Bruker Biospin/Avance III 400 MHz NMR spectrometer, respectively. Elemental analysis was carried out for all final compounds using an elemental analyser (Elementar vario MACRO cube). The synthetic procedures and analytical data for the products obtained in the intermediate steps are described in the supplementary information.

2.1.1. Synthesis of compound I

6-Hydroxynaphthalene-1-yl 2,4,5-trifluorobenzoate (**6**, 1.36 g, 4.28 mmol), compound **4** (2.34 g, 4.28 mmol) and 4-dimethylaminopyridine (DMAP, 0.06 g, 0.53 mmol) were mixed in CH_2Cl_2 (50 mL). The mixture was stirred at ambient temperature for 30 min under a nitrogen atmosphere. Subsequently, *N,N'*-dicyclohexylcarbodiimide (DCC, 0.88 g, 4.27 mmol) was added, and the reaction mixture was stirred at ambient temperature for 24 h under a nitrogen atmosphere. The precipitate of *N,N'*-dicyclohexylurea was removed by filtration. The filtrate was washed with a brine solution and water (three times), and the solvent was evaporated to dryness. The residue was chromatographed on silica gel using CH_2Cl_2. Recrystallisation from acetone afforded pure **I**. Yield: 32%; IR (KBr pellet, ν in cm^{-1}): 3061 (aromatic CH), 2913, 2847 (aliphatic CH), 1740 (conj. C = O), 1582, 1470 (aromatic C = C), 1435, 1344, 1273 (CO; CF); ^{1}H NMR (400 MHz, $CDCl_3$, δ in ppm): 8.42 (d, J = 10.5 Hz, 2H, ArH), 8.29 (d, J = 10.4 Hz, 2H, ArH), 8.17–8.13 (m, 2H, ArH), 8.01–7.98 (m, 2H, ArH), 7.84–7.63 (m, 2H, ArH), 7.56–7.34 (m, 7H, ArH), 7.09–6.96 (m, 3H, ArH), 4.04 (t, J = 6.5 Hz, 2H, OCH_2), 1.83–1.80 (m, 2H, OCH_2CH_2), 1.61–1.25 (m, 18H, CH_2), 0.86 (t, J = 6.6 Hz, 3H, CH_3); Anal. calcd. for $C_{50}H_{45}F_3O_9$: C 70.91, H 5.36; found: C 71.01, H 4.94.

2.1.2. Synthesis of compound IIa

Compound **IIa** was prepared in a similar manner to that described for the preparation of compound **I**. Quantities: 7-hydroxynaphthalene-2-yl 2,3,4-trifluorobenzoate (**7a**, 2.25 g, 7.07 mmol), compound **4** (3.87 g, 7.07 mmol), DMAP (0.11 g, 0.88 mmol) and DCC (1.46 g, 7.07 mmol). The product was chromatographed on silica gel using CH_2Cl_2. Recrystallisation from acetone afforded pure **IIa**. Yield: 44%; IR (KBr pellet, ν in cm^{-1}): 3122 (aromatic CH), 2913, 2848 (aliphatic CH), 1726 (conj. C=O), 1632, 1452 (aromatic C=C), 1287, 1165, 1057, 1028 (CO; CF); ^{1}H NMR (400 MHz, $CDCl_3$, δ in ppm): 8.34–8.28 (m, 4H, ArH), 8.14 (d, J = 8.9 Hz, 2H, ArH), 7.93 (d, J = 14.0 Hz, 2H, ArH), 7.70–7.69 (m, 2H, ArH), 7.41–7.34 (m, 6H, ArH), 7.16–7.09 (m, 2H, ArH), 6.98 (d, J = 14.4 Hz, 2H, ArH), 4.04 (t, J = 6.5 Hz, 2H, OCH_2), 1.89–1.78 (m, 2H, OCH_2CH_2), 1.48–1.16 (m, 18H, CH_2), 0.86 (t, J = 7.0 Hz, 3H, CH_3); Anal. calcd. for $C_{50}H_{45}F_3O_9$: C 70.91, H 5.36; found: C 70.66, H 5.42.

2.1.3. Synthesis of compound IIb

Compound **IIb** was prepared in a similar manner to that described for the preparation of compound **I**. Quantities: 7-hydroxynaphthalene-2-yl 2,4,5-trifluorobenzoate (**7b**, 2.11 g, 6.63 mmol), compound **4** (3.62 g, 6.63 mmol), DMAP (0.11 g, 0.83 mmol) and DCC (1.37 g, 6.63 mmol).

The product was chromatographed on silica gel using CH_2Cl_2. Recrystallisation from acetone afforded pure **IIb**. Yield: 46%; IR (KBr pellet, ν in cm^{-1}): 3081 (aromatic CH), 2913, 2852 (aliphatic CH), 1740 (conj. C=O), 1618, 1471 (aromatic C=C), 1282, 1253, 1166, 1059 (CO; CF); ^{1}H NMR (400 MHz, $CDCl_3$, δ in ppm): 8.31 (dd, J = 17.8, 8.8 Hz, 4H, ArH), 8.14 (d, J = 8.9 Hz, 2H, ArH), 8.01–7.92 (m, 3H, ArH), 7.69 (d, J = 2.0 Hz, 2H, ArH), 7.42–7.33 (m, 6H, ArH), 7.13–7.06 (m, 1H, ArH), 6.98 (d, J = 9.0 Hz, 2H, ArH), 4.05 (t, J = 6.4 Hz, 2H, OCH_2), 1.83–1.80 (m, 2H, OCH_2CH_2), 1.35–1.26 (m, 18H, CH_2), 0.87 (t, J= 6.6 Hz, 3H, CH_3); Anal. calcd. for $C_{50}H_{45}F_3O_9$: C 70.91, H 5.36; found: C 70.97, H 5.60.

2.1.4. Synthesis of compound IIc

Compound **IIc** was prepared in a similar manner to that described for the preparation of compound **I**. Quantities: 7-hydroxynaphthalene-2-yl 2,4,6-trifluorobenzoate (**7c**, 2.50 g, 7.86 mmol), compound **4** (4.30 g, 7.86 mmol), DMAP (0.12 g, 0.98 mmol) and DCC (1.62 g, 7.86 mmol). The product was chromatographed on silica gel using CH_2Cl_2. Recrystallisation from acetone afforded pure **IIc**. Yield: 43%; IR (KBr pellet, ν in cm^{-1}): 3076 (aromatic CH), 2918, 2843 (aliphatic CH), 1740 (conj. C=O), 1623, 1470 (aromatic C=C), 1258, 1237, 1166, 1125, 1049, 1013 (CO; CF); ^{1}H NMR (400 MHz, $CDCl_3$, δ in ppm): 8.29 (dd, J = 18.5, 7.8 Hz, 4H, ArH), 8.14 (d, J = 11.6 Hz, 2H, ArH), 7.93 (d, J = 8.8 Hz, 2H, ArH), 7.70 (dd, J = 6.0, 2.0 Hz, 2H, ArH), 7.42–7.34 (m, 6H, ArH), 6.98 (d, J = 8.8 Hz, 2H, ArH), 6.82 (t, J = 11.4 Hz, 2H, ArH), 4.04 (t, J = 6.6 Hz, 2H, OCH_2), 1.85–1.78 (m, 2H, OCH_2CH_2), 1.43–1.26 (m, 18H, CH_2), 0.87 (t, J = 6.6 Hz, 3H, CH_3); Anal. calcd. for $C_{50}H_{45}F_3O_9$: C 70.91, H 5.36; found: C 70.82, H 5.44.

2.1.5. Synthesis of compound IId

Compound **IId** was prepared in a similar manner to that described for the preparation of compound **I**. Quantities: 7-hydroxynaphthalene-2-yl 3,4,5-trifluorobenzoate (**7d**, 2.20 g, 6.91 mmol), compound **4** (3.78 g, 6.91 mmol), DMAP (0.11 g, 0.86 mmol) and DCC (1.43 g, 6.91 mmol). The product was chromatographed on silica gel using CH_2Cl_2. Recrystallisation from acetone afforded pure **IId**. Yield: 43%; IR (KBr pellet, ν in cm^{-1}): 3123 (aromatic CH), 2921, 2849 (aliphatic CH), 1731 (conj. C=O), 1573, 1462 (aromatic C=C), 1319, 1275, 1165, 1069, 1031, 1011 (CO; CF); ^{1}H NMR (400 MHz, $CDCl_3$, δ in ppm): 8.30 (dd, J = 17.6, 11.2 Hz, 4H, ArH), 8.14 (d, J = 11.6 Hz, 2H, ArH), 7.95–7.88 (m, 4H, ArH), 7.68 (dd, J = 9.6, 2.4 Hz, 2H, ArH), 7.42–7.31 (m, 6H, ArH), 6.98 (d, J = 2.0 Hz, 2H, ArH), 4.04 (t, J = 7.0 Hz, 2H, OCH_2), 1.83–1.79 (m, 2H, OCH_2CH_2), 1.48–1.22 (m, 18H, CH_2), 0.87 (t, J = 7.6 Hz, 3H, CH_3); Anal. calcd. for $C_{50}H_{45}F_3O_9$: C 70.91, H 5.36; found: C 71.09, H 5.36.

2.2. Mesophase characterisation

The transition behaviours were characterised by DSC (TA Instruments DSC Q2000). The DSC measurements were performed under a N_2 atmosphere with heating and cooling rates of 10°C/min. Optical texture observations were conducted using a polarising microscope (Carl Zeiss Axioskop 40 Pol; Nikon ME600) with a heating stage (Mettler FP82HT; Linkam LTS420).

Wide-angle X-ray diffraction (WAXD) experiments were conducted in the reflection mode with a Rigaku 12 kW rotating-anode X-ray ($Cu_{K\alpha}$ radiation) generator coupled with a diffractometer. The diffraction peak positions and widths were calibrated with silicon crystals in the high-2θ-angle region (>15°) and with silver behenate in the low-2θ-angle region. To monitor the structural evolution with temperature changes, a heating stage calibrated to be within an error of ±1°C was coupled to the diffractometer. Samples were scanned across a 2θ range of 1.5° to 35° at a scanning rate of 2°/min. Silicon crystal powder, which was used as an internal reference, shows a diffraction ring at a 2θ value of 28.466°. In the WAXD experiments, background scattering was subtracted from the sample scans.

Water-insoluble salts were filtered out of the tetrahydrofuran (THF) solution using a membrane filter. Subsequently, the filtrate was precipitated from water, collected by filtration, and dried under vacuum. The obtained LCs were injected between two indium tin oxide (ITO) glass slides by capillary action at 200°C. Each ITO glass slide, which had a square patterned electrode and an area of 1 cm^2, was spin-coated with a commercial planar alignment reagent (JSR). The spin-coated alignment layer was pre-baked at 100°C for 10 min to evaporate the solvent and then cured at 210°C for 1 h to complete the imidisation reaction. The cell thickness was maintained using glass spacers 5 μm in diameter. The temperature of the cell was maintained within an accuracy of 0.1°C using a heating stage (Mettler FP90). Spontaneous polarisations were measured using the triangular-wave method [35], whereby it is easy to subtract the background current. The polarisation current, converted into a voltage signal through a current amplifier (Keithley Model 428), was measured with a digitising oscilloscope (Tecktronix TDS-754D).

3. Results and discussion

Compounds **I** and **IIa-d** were synthesised by Steglich esterification followed by Jones oxidation. We sought to make a highly polarisable, trans-conformational system to maximise the net dipole moment for the long arms. Therefore, we adopted an elongated arm consisting of a naphthalene and three phenyl rings connected with ester linkages along one *p*-direction. Initially, we struggled with whether the substitution position of the naphthalene central core should be the asymmetric 1,6-position (**I**) or the symmetric 2,7-position (**IIa–d**) in order to induce macroscopic polar symmetry. However, in this study, we could quickly determine that a molecule with asymmetric 1,6-naphthalene substitution was not liquid crystalline (**I**: T_m = 185°C; ΔH_m = 45.0 kJ mol^{-1}). Hence, herein we focused on structures with symmetric 2,7-naphthalene substitution. Moreover, the short arm was composed of only one phenyl ring with 2,3,4-, 2,4,5-, 2,4,6- or 3,4,5-trifluoro substituents, which might be the origin of the net dipole moment owing to its high electronegativity. At the molecular structural level, the substitution pattern of the tri-fluorinated phenyl group was considered from two structural viewpoints. The first is whether the substitution position is 'symmetric' (i.e., the 2,4,6- and 3,4,5-positions) or 'non-symmetric' (i.e., the 2,3,4- and 2,4,5-positions). The second is whether the substitution pattern is 'continuous' (i.e., the 2,3,4- and 3,4,5-positions) or 'non-continuous' (i.e., the 2,4,5- and 2,4,6-positions).

Types of mesophases and phase transitions have been assigned in the base of DSC, POM and XRD results with reference to the literature [10–34]. Summarising, compound **IIa** forms six different mesophases including a monotropic unknown smectic phase and a hexatic-type smectic phase, that is, Iso ↔ N_{CybC} ↔ SmA ↔ SmC_s ↔ SmC_a (→ SmX) ↔ Cr (← HexI). Compound **IIb** forms four different enantiotropic fluid mesophases and one hexatic-type smectic phase, that is, Iso ↔ N_{CybC} ↔ SmA ↔ SmC_s ↔ SmC_a ↔ Cr (← HexI). Compound **IIc** forms three different fluid mesophases including a monotropic anticlinic SmC phase, that is, Iso ↔ N_{CybA} ↔ SmA (→ SmC_a) ↔ Cr. Compound **IId** forms four different enantiotropic fluid mesophases and one hexatic-type smectic phase, that is, Iso ↔ SmA ↔ SmC_s ↔ SmC_a ↔ Cr (← HexI).

3.1. Thermal and microscopic behaviour

Figure 1 presents the DSC thermograms of compounds **II**. All compounds are thermally stable as confirmed by the reproducibility of the thermograms on the second heating and cooling cycles. The thermograms reveal that: (i) on heating, **IIa, IIb** and **IId** show two distinct melting peaks, whereas **IIc** exhibited only one distinct melting peak; (ii) on cooling, **IIa, IIb** and **IId** show a sharp, strong peak for crystallisation, whereas **IIc** exhibited multiple peaks for crystallisation; (iii) on both heating and cooling, **IIa, IIb** and **IIc** showed a small peak for isotropisation, whereas **IId** showed a medium peak for isotropisation; (iv) for all compounds, the peaks for mesophase-to-mesophase transitions were exceedingly small but accurately defined.

The transition temperatures (°C) and the associated enthalpies (kJ mol^{-1}) obtained from the DSC thermograms of compounds **II** are listed in Table 1. All the compounds had melting temperatures (m.p.) in the range of 148°C to 161°C depending on the structure. On cooling, all the compounds showed supercooling phenomena and had crystallisation temperatures in the range of 124–136°C. The isotropisation temperatures (T_i) of all compounds except **IIb** were in the range of 222–224°C. The T_i of compound **IIb** was lower than other compounds by approximately 10°C. This could be ascribed to the shorter persistence length of the molecules in the fluid state, described in the next section, which was probably due to the non-continuous, non-symmetric 2,4,5-substitution pattern of the F atoms. On cooling, compound **IIa** formed a nematic phase at 223°C, a SmA phase at 210°C, and a SmC phase at 196°C. The nematic phase could be assigned as a SmC-type cybotactic nematic phase (N_{CybC}) because the enthalpy change for the Iso-to-N transition (ΔH = 0.30 kJ mol^{-1}) is comparable with the reported values for the Iso-to-N_{CybC} transition for HSLCs [20]. At 188°C, the SmC_s-to-SmC_a transition was distinguished by a distinct enthalpy change (ΔH = 0.12 kJ mol^{-1}). A transition from the SmC_a phase to SmX phase occurred at 135°C with an enthalpy change (ΔH = 0.12 kJ mol^{-1}) comparable with the enthalpy changes for transitions between two different fluid smectic phases for HSLCs [19]. In the second heating cycle, this compound exhibited a Cr-to-HexI transition at 145°C, which occurred on the first heating scan at 108°C. Upon further heating, four transitions occurred reversibly at the corresponding temperatures and with equivalent enthalpy changes as the values obtained from the cooling cycle. The DSC results of compound **IIb** reveal a similar behaviour as compound **IIa**. The key difference is that the former did not exhibit an exotherm for the SmC_a-to-SmX transition on cooling. Compound **IIc** formed a nematic phase at 223°C on cooling and showed a transition into SmA phase at 175°C. The enthalpy change for the Iso-to-N transition for this compound (ΔH = 0.72 kJ mol^{-1}) was more than twice those for **IIa** and **IIb**. This suggests that the nematic phase can be assigned to be the SmA-type cybotactic nematic phase (N_{CybA}) [19]. In addition, this

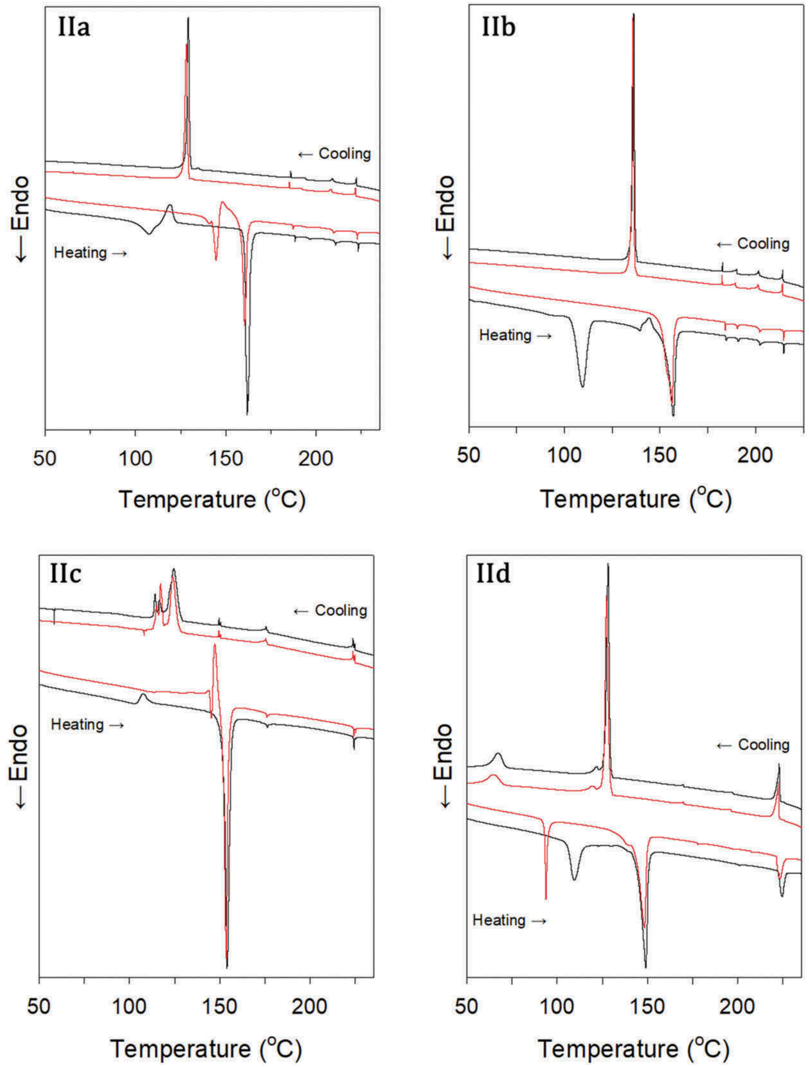

Figure 1. (Colour online) DSC thermograms on heating and cooling cycles (rate = 10°C/min). The red curves indicate the second DSC scan.

compound showed a monotropic transition from SmA to $\mathrm{SmC_a}$ at 149°C and the enthalpy change (ΔH = 0.20 kJ $\mathrm{mol^{-1}}$) was comparable to the corresponding transitions for **IIa** and **IIb**. Interestingly, compound **IId**, with the continuous, symmetric 3,4,5-substitution position of F atoms, shows quite different mesogenic behaviour from the rest of the compounds. For example, on cooling, the ΔH for isotropisation (3.0 kJ $\mathrm{mol^{-1}}$) of **IId** was approximately ten times higher than those of the other compounds (ca. 0.3 kJ $\mathrm{mol^{-1}}$). This suggests that an Iso-to-SmA transition takes place. Upon further cooling, the SmA-to-$\mathrm{SmC_s}$ and $\mathrm{SmC_s}$-to-$\mathrm{SmC_a}$ transitions were observed at 197°C and 170°C, respectively, with a small but distinct enthalpy change. On first heating, this compound formed one HexI phase at 109°C in addition to the three different types of enantiotropic fluid smectic phases.

Figures 2 and 3 present the optical textures of the mesophases observed using ordinary microscopy slides. On heating, compound **IIa** formed four different smectic phases in sequence before forming one nematic phase. Above the melting point defined by DSC, at 172°C the $\mathrm{SmC_a}$ phase is observed as a Schlieren texture with four brush defects, [*s*] = 1 (Figure 2(a)). A transition between the $\mathrm{SmC_a}$ phase and the $\mathrm{SmC_s}$ phase is started at 185°C; this was apparent from the conversion of the birefringent texture of $\mathrm{SmC_a}$ into a pseudo-isotropic texture typical of $\mathrm{SmC_s}$ (Figure 2(b)), which is optically uniaxial and thus can only be detected by using a compensator, which gives a brownish dark texture. Upon further heating, this compound formed SmA phase and $\mathrm{N_{Cyb}}$ phase in sequence. These two phases also appeared as pseudo-isotropic phases. It is inferred that the $\mathrm{SmC_s}$, SmA and $\mathrm{N_{Cyb}}$ phases might form dark conglomerate (DC) phase due to the quasi-bent-shaped conformation of molecules [36]. The textural changes between those three dark phases are very subtle. Upon cooling from the isotropic liquid, four enantiotropic phases appeared. As the temperature was lowered, the N_{Cyb}, SmA and SmC_s phases in sequence appeared as dark phases. At even lower temperatures, a Schlieren texture with two brush defects, [*s*] = 1/2 (Figure 2(c)) was observed, which was attributed to the SmC_a phase, and this converted paramorphically to a fan-shaped texture as the temperature was lowered further (Figure 2(d)). On further cooling, a dark phase grows from the SmC_a phase (Figure 2(e)), which is a monotropic smectic phase (SmX). This dark phase can be excluded as being related to the hexatic phase because the enthalpy change for this transition is comparable with those for fluid smectic phases. After the transition to the crystal phase, a fan-shaped texture with concentric arcs develops from the dark texture (Figure 2(f)), which changed into a fan-shaped texture of a HexI phase on the second heating cycle (Figure 2(g)).

The POM observations of compound **IIb** reveal a similar series of phases as for compound **IIa** except for the monotropic SmX phase. That is, the N_{Cyb}, SmA and SmC_s phases are optically uniaxial at higher temperatures, whereas as the temperature is lowered, the SmC_a phase appears with a texture in which Schlieren and homogeneous regions coexist (Figure 2(h)).

Compound **IIc** formed two different enantiotropic phases (N_{Cyb} and SmA) and one monotropic phase (SmC_a) in sequence. The nematic phase appeared with a Schlieren texture (Figure 3(a,f)) at higher temperature. Subsequently, upon cooling, an enantiotropic SmA phase appeared can be identified from the weak birefringence texture, which consists of either broad domain-like areas (Figure 3(b,e)) or sharp fingerprint-like patterns (Figure 3(c)). At even lower temperatures, the monotropic SmC_a phase appears as a Schlieren texture (Figure 3(d)).

Compound **IId** formed three different types of fluid smectic phases and, interestingly, an additional HexI phase. The SmA phase appeared at higher temperatures as a completely dark pseudo-isotropic texture. Upon cooling, in the same sample region, a fan-shaped texture with focal conics for the SmC_s phase (Figure 3(h)) grew from the pseudo-isotropic melt through the growth of bâtonnets (Figure 3(g)). Upon further cooling, the same sample region changed to a broken fan-shaped texture for the SmC_a phase (Figure 3(i)). At even lower temperatures, the crystal phase appeared as a fan-shaped texture with an equidistant line pattern (Figure 3(j)). On reversing the process through heating the sample, the SmC_a phase appeared with a poorly developed focal-conic-like texture (Figure 3(k)). Subsequently, the SmC_s phase appeared with a typical focal-conic texture upon further heating and the pseudo-isotropic region developed from this texture at yet lower temperature than the SmA phase (Figure 3(l)).

Table 1. Transition temperatures (*T*, °C) and enthalpy changes (Δ*H*, kJ mol^{-1} in parentheses).

Code[a]	DSC scan[b]	m.p.	HexI	SmX	SmC_a	SmC_s	SmA	N_{Cyb}	Iso
IIa (2,3,4-)	1–h	161 (37.7)	● 108 (20.0)		● 188 (0.12)	● 196 (0.08)	● 210 (0.27)	● 223 (0.30)	●
	1–c	130 (20.7)		● 135 (0.12)	● 186 (0.12)	● 194 (0.06)	● 209 (0.25)	● 222 (0.30)	●
	2–h	160 (21.9)	● 145 (11.6)		● 187 (0.12)	● 194 (0.10)	● 209 (0.29)	● 222 (0.29)	●
IIb (2,4,5-)	1–h	156 (19.2)	● 109 (21.4)		● 184 (0.13)	● 191 (0.10)	● 202 (0.23)	● 214 (0.24)	●
	1–c	136 (21.0)			● 182 (0.12)	● 190 (0.17)	● 201 (0.25)	● 214 (0.25)	●
	2–h	156 (22.5)			● 184 (0.13)	● 190 (0.14)	● 202 (0.27)	● 214 (0.26)	●
IIc (2,4,6-)	1–h	153 (37.4)					● 176 (0.16)	● 224 (0.34)	●
	1–c	114, 117, 124 (11.6)[c]			● 149 (0.20)		● 175 (0.37)	● 223 (0.72)	●
	2–h	146, 153 (33.1)[c]					● 176 (0.16)	● 224 (0.38)	●
IId (3,4,5-)	1–h	149 (26.1)	● 109 (9.9)		● 178[d]	● 200 (0.14)	● 224 (3.1)		●
	1–c	68, 128 (25.5)[c]			● 170 (0.11)	● 197 (0.15)	● 222 (3.0)		●
	2–h	93, 148 (22.6)[c]			● 178 (0.02)	● 198 (0.01)	● 223 (3.0)		●

[a] Numbers in parentheses stand for the substitution position of the trifluoro substituents.
[b] Abbreviations: 1–h = first heating scan; 1–c = first cooling scan; 2–h = second heating scan.
[c] Total enthalpy change for multiple melting or multiple crystallisation processes.
[d] The transition without detectable enthalpy was confirmed by microscopic observation.

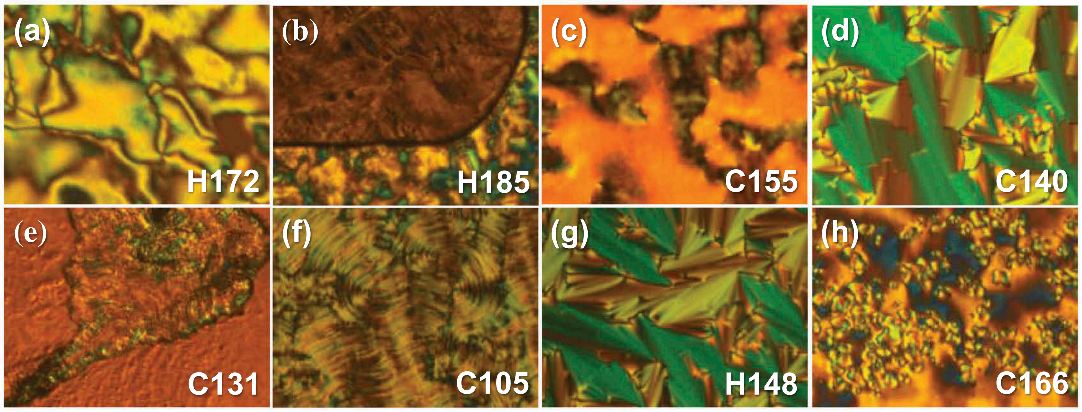

Figure 2. (Colour online) POM images observed for **IIa** (a–g) and **IIb** (h) at the indicated temperatures (abbreviations: H = heating; C = cooling). Images were recorded using ordinary microscopy slides; magnification 200× except for (b) and (e) (100×); a 1/4λ compensator was used for all observations.

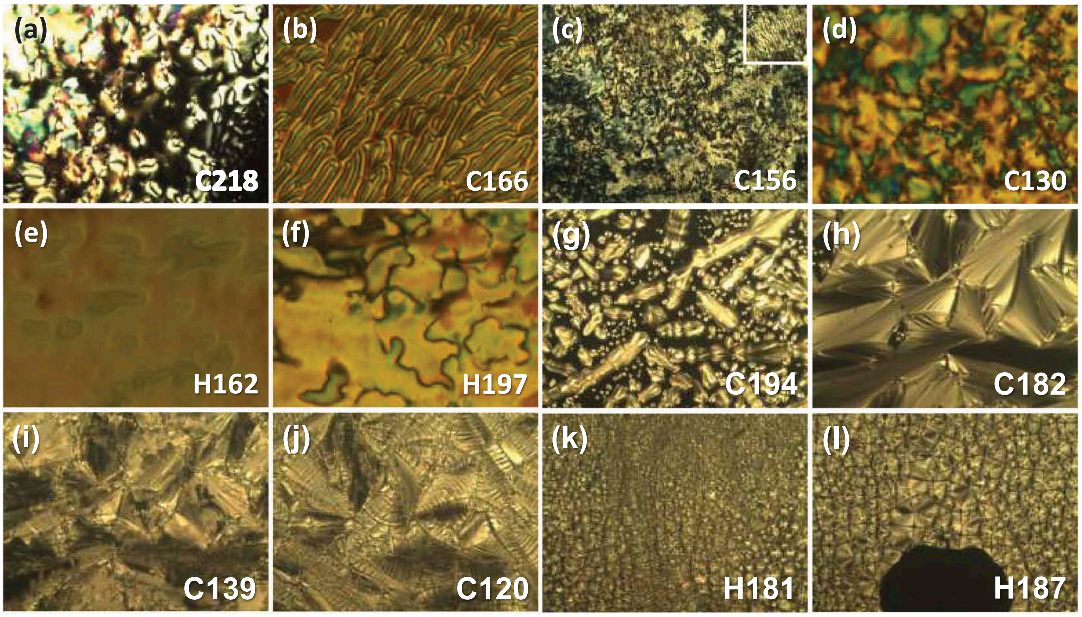

Figure 3. (Colour online) POM images observed for **IIc** (a–f) and **IId** (g–l) at the indicated temperatures (abbreviations: H = heating; C = cooling). Images were recorded using ordinary microscopy slides; magnification 200×; a 1/4λ compensator was used for (b), (d), (e) and (f); the inset shows the enlarged fingerprint pattern.

3.2. X-ray diffraction properties

Figure 4 presents the XRD patterns obtained for compounds **II** at the indicated temperatures. At room temperature, all compounds show a number of fairly sharp reflections, which is indicative of the crystal phase. On heating yet below the m.p., all compounds except **IIc** exhibit fairly sharp reflection patterns, which are different from the patterns of the crystal phases. This suggests a smectic phase possessing in-plane positional order (HexI phase). In the small-angle region, compound **IIa** shows two strong reflections at d_1 = 4.25 nm and d_2 = 2.19 nm in the crystal phase, and at d_1 = 3.99 nm and d_2 = 1.99 nm in the HexI phase. This means that upon heating the crystal lamellar phase, which is prepared by non-solvent precipitation during the synthetic procedure, can be converted into the smectic lamellar phase. A further increase in temperature resulted in a significant difference in the diffraction pattern between the first and second smectic phases, with the fluid phases showing only two reflections. The SmC_a phase of **IIa** has a diffuse wide-angle peak at approximately 0.46 nm, which is indicative of the

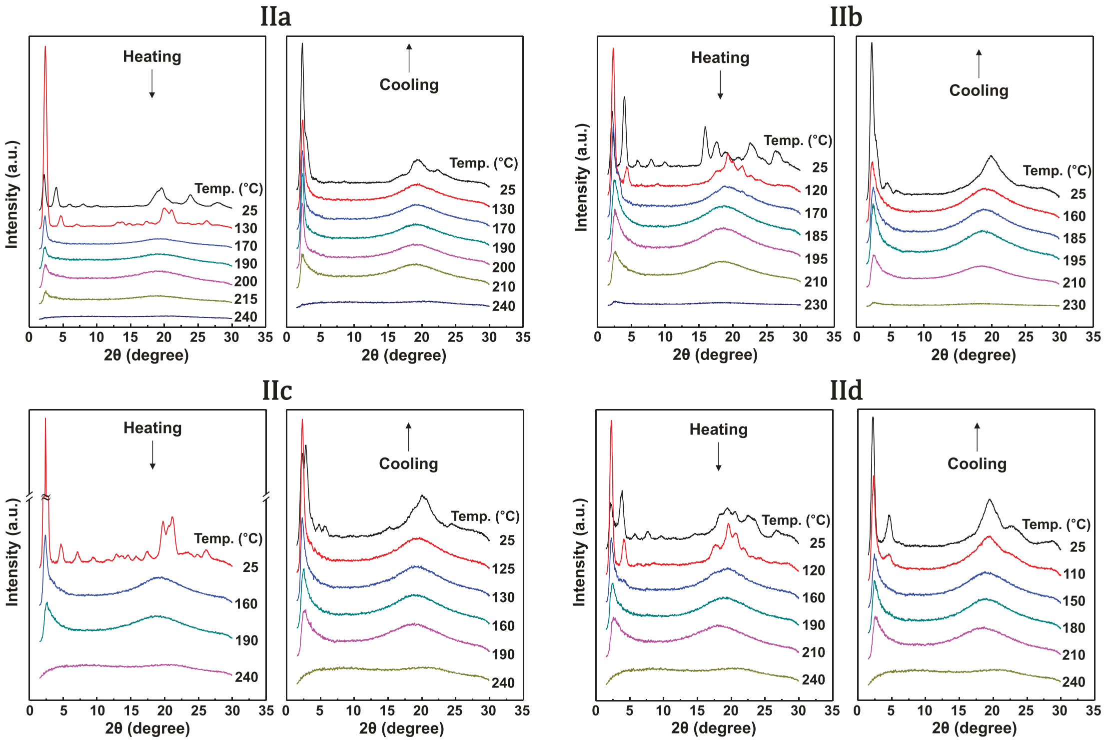

Figure 4. (Colour online) Sets of XRD patterns on heating and cooling scans. The *d* values (nm) obtained on cooling at the indicated temperatures are: **IIa**: 4.25, 3.99, 3.81, 3.71, 3.61 and 3.36; **IIb**: 4.19, 3.81, 3.67, 3.52 and 3.31; **IIc**: 4.39, 4.33, 4.22, 3.73, 3.55 and 3.34; **IId**: 4.37, 4.31, 3.69, 3.62 and 3.52.

longitudinal chain packing disappearing. In its small-angle region, a fairly strong peak appears at 3.81 nm, which suggests short-range layer periodicity. For the fluid smectic phases, on sequential transition from SmC_a to SmC_s and from SmC_s to SmA, the layer spacing decreased slightly (by approximately 0.1 nm for each transition). Upon these successive transitions, the high angular reflection did not show any significant change. At higher temperature, the *d* value of the nematic phase decreased by 0.25 nm. Nevertheless, there was no significant difference in the diffraction patterns between the fluid smectic phases and the nematic phase. This means that the smectic-like short-range order of the molecules is retained within the nematic clusters. On cooling, compound **IIa** showed four reflection patterns corresponding to four different enantiotropic mesophases. Upon further cooling, a reflection for an additional fluid smectic phase (SmX) was observed at 130°C. However, upon lowering temperature further, no patterns for the HexI phase were observed, although it appeared on the second heating cycle (see Figure S1, ESI).

The X-ray reflection patterns of compound **IIb** showed similar results as those observed for **IIa** with the same phase sequence except for the monotropic SmX phase. The lower *d* values of **IIb**, with the non-continuous, non-symmetric 2,4,5-trifluorophenyl substitution pattern, compared with **IIa**, with the continuous, non-symmetric 2,3,4-trifluorophenyl substitution pattern, can be attributed to the shorter effective molecular length due to the decreased bending angle of the molecules.

On heating, compound **IIc**, with the non-continuous, symmetric 2,4,6-trifluorophenyl group substitution position, exhibited only low-ordered X-ray patterns corresponding to two different fluid smectic phases and one nematic phase, dissimilar to the above-mentioned compounds. The similarity of *d* value of its nematic phase to those of **IIa** and **IIb** considerably burdens the assignment of the N_{CybA} phase although the ΔH for the N-to-SmA phase transition of the former compound was significantly higher than those of the latter compounds. The *d* values of the smectic phases at 160°C (3.55 nm) and at 130°C (3.73 nm) were comparable to those for the SmA phase (avg. 3.55) and the SmC_a phase (avg. 3.77) rather than the SmC_s phase (avg. 3.67) of other compounds.

At room temperature, compound **IId** showed two strong reflections at d_1 = 4.37 nm and d_2 = 2.23 nm in the small-angle region, attributed to the solid-state crystal lattice structure. As the temperature increased, in the wide-angle region, the HexI phase appeared with a significantly different pattern to that of the crystal lattice, and in the small-angle region, two reflections at d_1 = 4.22 nm and d_2 = 2.12 nm were observed. A further increase in temperature resulted in the fluid smectic phases, the patterns of which showed a broad diffraction in the wide-angle region, and the d value significantly decreased by 0.62 nm in the small-angle region. This indicates a transition from the HexI to the SmC phase. As the temperature further increased, the d value decreased slightly (by 0.07 nm), suggesting a transition from the SmC_a to the SmC_s phase. At high temperature, the d value becomes 3.52 nm, which more closely resembles the typical values for the SmA phase rather than the N_{Cyb} phase (avg. 3.34) for other compounds.

Figure 5 presents the temperature dependence of the layer spacing. Upon cooling, clear discontinuities are observed in the layer spacing and thus the phase transitions are clearly perceivable: a jump in the layer spacing is observed at the phase transition, whereas a very subtle or slight increase is observed within the temperature range of each phase, regardless of the type of phase. Specifically, the crystal and HexI phases have relatively large d values (3.99–4.39 nm), whereas the fluid smectic and cybotactic nematic phases have relatively smaller d values (3.31–3.81 nm). Overall, the d values obtained on cooling increased with the temperature, giving variations of less than 5% for the fluid states. The difference in the d values might result from a change of the molecular conformation or either a change of the tilt or degree of intercalation. Herein, the pseudo-rod-like molecules should lead to a considerably smaller change in the molecular conformation compared with BCLCs. Previously, we reported that the molecular length (l) for analogous molecules with energy minimised conformations was estimated to be 4.2 nm, based on the assumption that there was no intercalation between chains [27]. In this study, the 1,3-phenylene central core used previously was replaced with the 2,7-naphthalene central core, and the l value was estimated to be 4.38 nm by using the MM2 element of the ChemDraw3D software. Herein, the fluid smectic phases formed layers with d/l = 0.80–0.87. In particular, an unexpected decrease of the d value is noted for the transition into the non-tilted SmA phase and thus the tilt angle cannot be estimated by using the ratio d_{SmC}/d_{SmA}. This strongly suggests that the smectic phases do not represent simple single layer structures, but must be considered as significantly interdigitated double layer structures. Moreover, we assumed that the quasi-bent-shaped molecules with a highly polar end group would lead to an abrupt change in the molecular arrangement

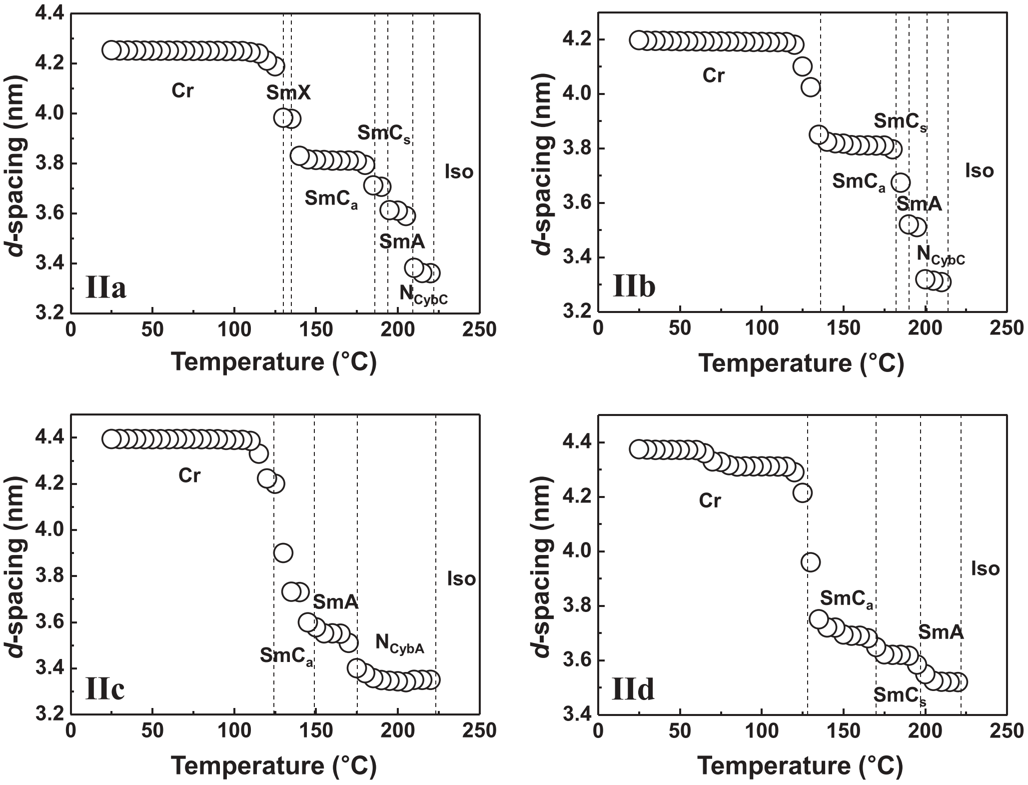

Figure 5. (Colour online) Temperature dependence of the d value of the small-angle reflection in the different mesophases during cooling. The dashed lines indicate the transition temperatures determined from DSC measurements.

between the polar packing and the aliphatic-aliphatic intercalation [19].

3.3. Surface alignment and E-O behaviour

Figure 6 presents the optical textures observed for compounds **II** using a planar cell. The crystal state of **IIa** displayed negligible alignment in rubbed polyimide (PI) coated cells (Figure 6(a)). On heating, its HexI phase (Figure 6(b)) as well as the SmC$_a$ phase (Figure 6(c,d)) presented distinctly oriented textures with broken-fan-like domains along the rubbing direction. Upon further heating, both the SmC$_s$ (Figure 6(e)) and SmA (Figure 6(f,g)) phases surprisingly showed uniform textures, which converted into a pseudo-isotropic texture upon transition to the N$_{CybC}$ phase (Figure 6(h)). Possibly, this completely dark phase could be the dark conglomerate (DC) phase resulting from distortion of the long-range periodic order. The crystal phase of **IIb** had a striped pattern aligned along the rubbing direction (Figure 6(i)). This implies that in the cell fabrication process, the director of the smectic phase can be preserved during the crystallisation of the melt. Upon heating, the SmC$_a$ phase of **IIb** displayed a uniform texture (Figure 6(j)), which started to change into the dark phase at 170°C (Figure 6(k)). As the temperature increased this dark phase was persisted till isotropisation (Figure 6(l)). Similar to **IIb**, compound **IIc** showed a striped pattern along the rubbing direction for the crystal phase (Figure 6(m)), and subsequently exhibited uniform textures for both the SmA (Figure 6(n,o)) and N$_{CybA}$ (Figure 6(p–r)) phases, which converted into the dark phase at higher temperature (Figure 6(s)). Dissimilar to other compounds, compound **IId** showed no planar alignment along the rubbing direction in any of the birefringent phases. However, at higher temperature, the SmC$_a$ phase appeared along with the dark phase (Figure 6(t)).

Interestingly, the colour of the homogeneous images changed with temperature. Compounds **IIa** (Figure 6(e–g)) and **IIb** (Figure 6(j,k)) showed a red-shifted colour change whereas compound **IIc**

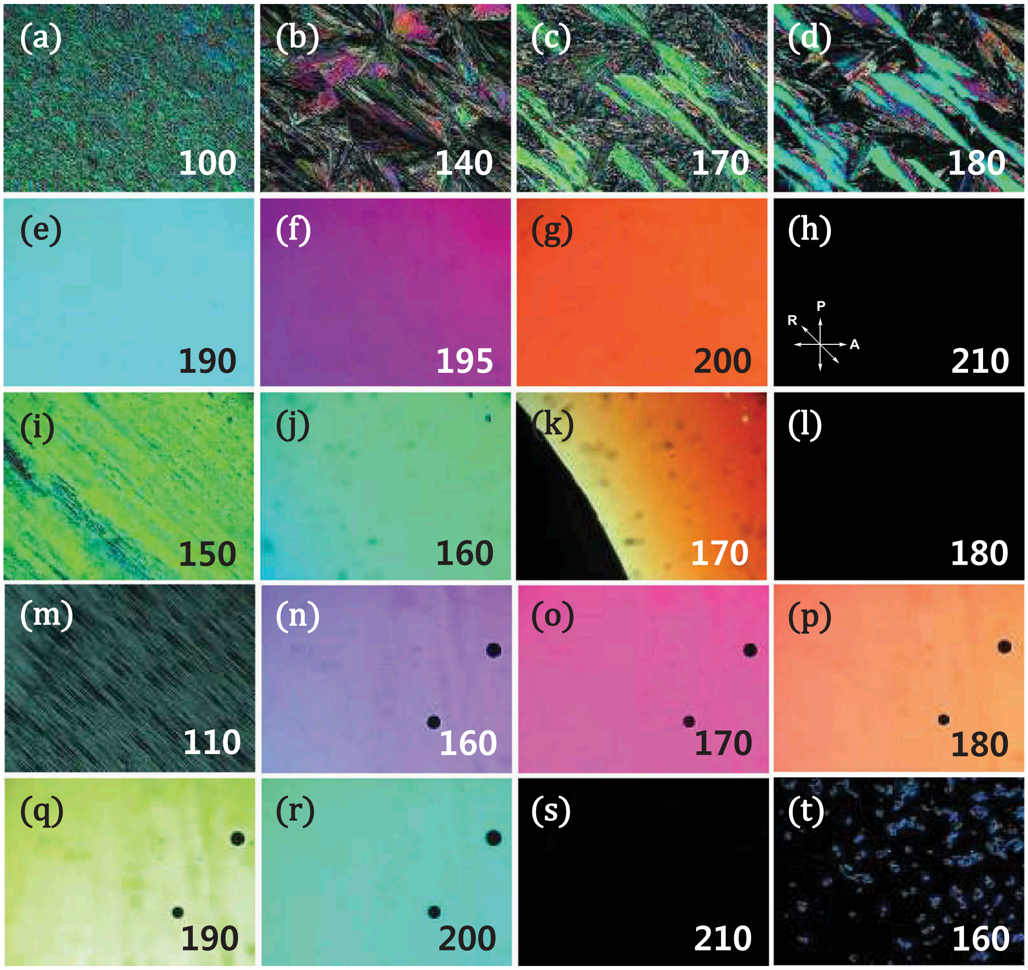

Figure 6. (Colour online) POM images at the indicated temperatures (°C) recorded from samples in 5 μm planar alignment cells. The upper rubbing direction was antiparallel to the lower rubbing direction. The polariser (P) meets at right angles to the analyser (A), which makes an angle of ± 45° with the rubbing direction (R). (a–h) **IIa**; (i–l) **IIb**; (m–s) **IIc**; (t) **IId.**

(Figure 6(n–r)) exhibited a blue-shifted colour change. Shanker et al. reported that for optically uniaxial smectic phases of BCLCs in a planar cell, the colour change was a result of an increase in the order parameter as the temperature increased [37]. Herein, at the quarter-wavelength retardation condition, the maximum transmittance wavelength is different from the incident wavelength depending on the given thickness. Nonetheless, the cell thickness was maintained using glass spacers 5 µm in diameter and thus, this factor might scarcely affect the interpretation of the colour changes in birefringence depending on the temperature.

For the detection of the polar character of the mesophases, all compounds **II** were purified by using the method described in the Experimental section in order to get rid of ionic impurities. Figure 7 presents polarisation current graphs measured by using a triangular-wave method, which were scaled to the same amplitude for ease of comparison. The current slopes were found to gradually increase with increasing temperature as the ionic mobility also increased in the mesogenic phase (see insets in Figure 7). For all compounds except for **IId**, distinct single reverse current peaks appeared with every half period of the applied triangular wave voltage. For **IIa** and **IIc**, distinct single reverse current peaks were observed over the full temperature range of the smectic phases. As the temperature increased, the reverse current peaks of **IIa** increased steadily, whereas the reverse current peaks of **IIc** decreased distinctly. This means that, as the temperature increases, for **IIa** the polar character slightly increases with the sequential SmC$_a$–SmC$_s$–SmA phase transitions, whereas for **IIc** the polar character of the SmA phase clearly decreases. On heating, compound **IIb** exhibited relatively broad reverse current peaks only in the temperature range corresponding to the SmC$_a$ phase. After the transition to the SmC$_s$ phase at T = 184°C defined by DSC, no current responses were observed in the temperature range related to the both of SmC$_s$ and SmA phases. This indicates that the SmC$_a$ phase of **IIb** could possess relatively weak polar character but the remaining two smectic phases did not at all. For compound **IId**, no remarkable current peaks were observed within the total measured temperature range for the smectic phases. This indicates that compounds **IIa, IIb** and **IIc** can form SmP$_F$ phases (i.e., ferroelectric phases), whereas compound **IId** cannot.

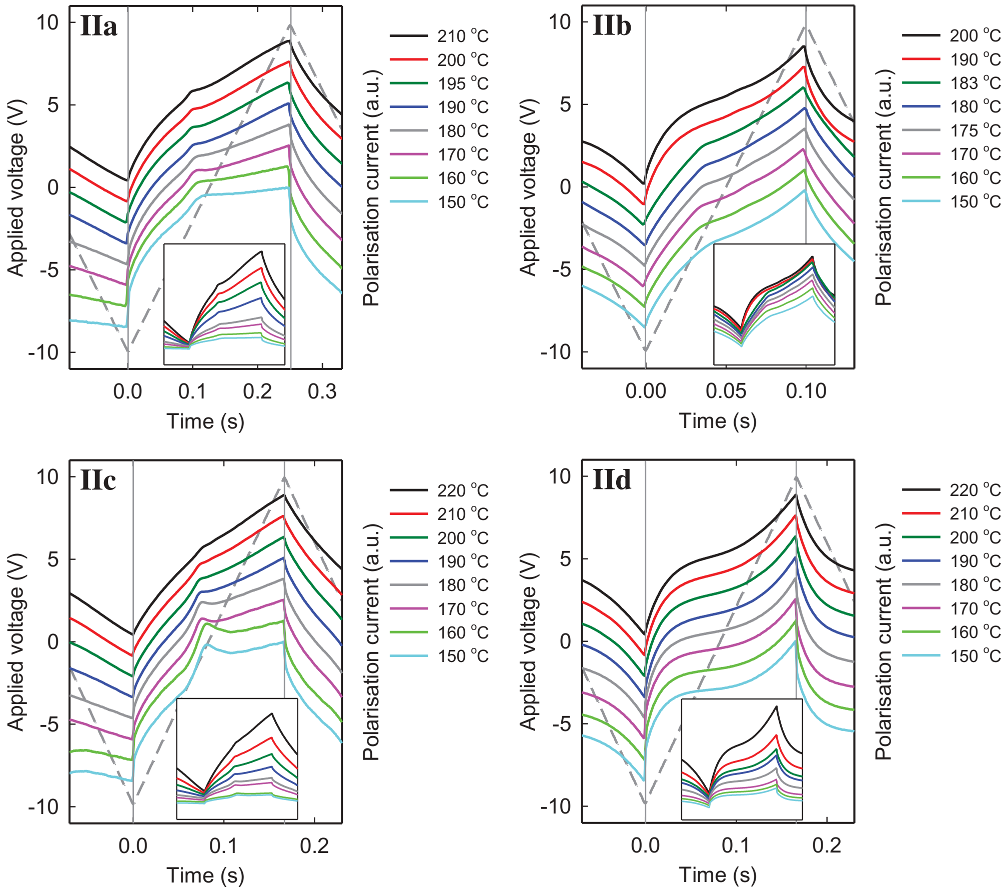

Figure 7. (Colour online) Switching current response obtained by applying a triangular voltage (E = 1.0 V µm^{-1}) at the indicated temperatures.

4. Conclusions

A new series of the HSLCs-3 were synthesised and characterised, which we called the either quasi-BCLCs or pseudo-RLLCs. Herein, adoption of the 2,7-naphthalene central cores as well as tri-fluorinated phenyl terminal was beneficial for elucidating the origin of polar symmetry. Our intention is to induce macroscopic polarity along tip direction due to highly polar symmetry in spite of remarkably short ‘arm’ with no flexible terminal chains. We suggest a strongly interdigitated double-layered structure instead of a monolayer structure in the fluid smectic phases, as the *l* values are substantially larger than the *d* values. Interestingly the new HSLCs-3 formed the SmC_a phase and SmC_s–SmC_a transitions, which are frequently observed in BCLCs [36] and HSLCs [6–11,19,20] rather than RLLCs. In addition, the HSLCs-3 revealed various mesomorphic polymorphisms depending on the substitution pattern of the three fluorine atoms (Figure 8). In summary, **IIa** with a continuous, non-symmetric 2,3,4-substitution position showed hexamorphism including a monotropic SmX phase on cooling and a HexI phase on heating; **IIb** with a non-continuous, non-symmetric 2,4,5-substitution position showed tetramorphism enantiotropically and an additional HexI phase upon heating; **IIc** with a non-continuous, symmetric 2,4,6-substitution position showed trimorphism including a monotropic SmC_a phase; **IId** with a continuous, symmetric 3,4,5-substitution position showed trimorphism enantiotropically and an additional HexI phase upon heating. Surprisingly, in the ordinary microscopy slides, the DC phases appeared in the SmC_s, SmA and N_{CybC} for both of **IIa** and **IIb**, and in the SmA of **IId** (Figure 8(b,c)). In the planar alignment cells, compound **IIc** showed a DC phase in the N_{CybA} phase (Figure 8(a)). This means that some mesophases can have a distortion of the long-range periodic order. Interestingly, the crystal phases of **IIb** and **IIc** showed the homogeneously aligned textures with striped pattern along the rubbing direction, and the SmC_a and HexI phases of **IIa** exhibited the heterogeneously aligned textures with a broken-fan-shaped defect along the rubbing direction. Moreover, the SmC_s and SmA phases of **IIa**, the SmC_a phase of **IIb**, and the SmA phase of **IIc** showed the completely homogeneous (i.e., uniform) texture under the planar boundary conditions. These results confirm that the HSLCs-3 can manifest the good alignment characteristics in the planar anchoring conditions, which is a typical feature of RLLCs. More noteworthy is that all the pseudo-rod-like molecules except **IId** show distinct reverse currents in some fluid smectic phases when using the triangle-wave method. This provides the first experimental evidence that non-chiral HSLCs-3 with a quasi-bent conformation can form a polar fluid smectic phase. Considering the molecular geometry, it is not surprising that the conventional HSLCs (HSLCs-1 and 2) can form a polar mesophase because both of the arms are long enough to construct the bent shape needed. On the other hand, it is astonishing that the third type of HSLCs (HSLCs-3) can form a polar mesophase because one of the arms is too short to have an effective bent shape and thus may have an almost linear shape. Furthermore, we have postulated that the monotropic SmX phase of **IIa**, which occurred at a lower temperature than the SmC_a phase, could be a heliconical smectic

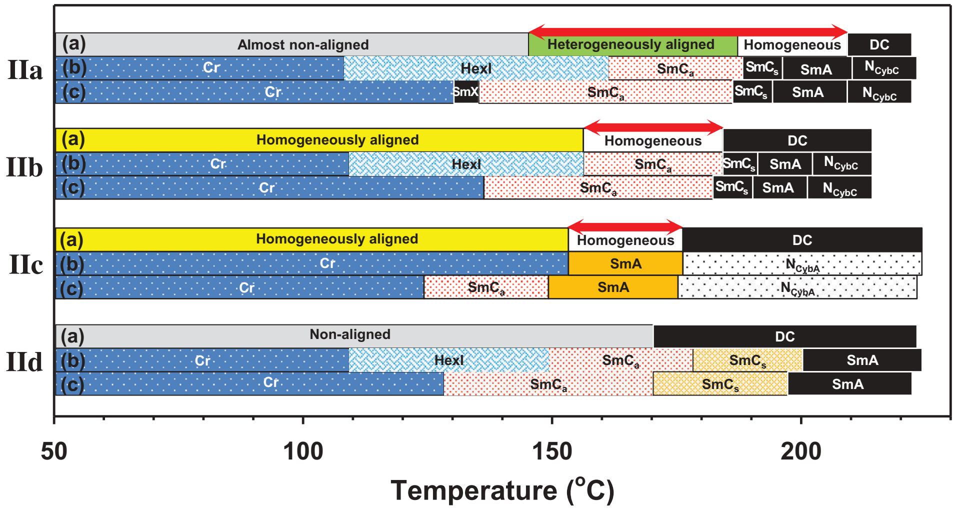

Figure 8. (Colour online) Orientation and phase transition behaviour depending on the molecular and cell structure. The red arrows indicate the existence of polar mesophases, and the black bars stand for DC phases: (a) planar alignment cell; ordinary glass slide on first heating (b) and on cooling (c).

phase (SmC_{TB}) [3]. This might be attributed to the interdigitated bilayer structure as a result of the existence of a strong polar head group on the short arm of the pseudo-rod-like molecules. However, future studies will be required to ascertain the assignment of such SmC_{TB} phase. In conclusion, it is our belief that the newly synthesised HSLCs-3 are efficacious in manifestation of the truly intermediate mesomorphism that can form either polar packing similar to BCLCs or bookshelf packing similar to RLLCs depending on the temperature and anchoring conditions.

Disclosure statement

No potential conflict of interest was reported by the authors.

Funding

This research was supported by the Basic Science Research Program (No. NRF-2017R1D1A1B03030179) through the National Research Foundation of Korea (NRF) grants funded by the Korea government (MSIP).

References

[1] Tschierske C. Mirror symmetry breaking in liquids and liquid crystals. Liq Cryst. 2018;45:2221–2252.

[2] Walba D. Ferroelectric liquid crystal conglomerates. In: Green M, Nolte R, Meijer E, editors. Materials-chirality. Vol. 24. New Jersey: John Wiley & Sons, Inc; 2003. p. 457–518.

[3] Abberley JP, Killah R, Walker R, et al. Heliconical smectic phases formed by achiral molecules. Nat Commun. 2018;9:228;1–7.

[4] Niori T, Sekine T, Watanabe J, et al. Distinct ferroelectric smectic liquid crystals consisting of banana shaped achiral molecules. J Mater Chem. 1996;6:1231–1233.

[5] Link DR, Natale G, Shao RF, et al. Spontaneous formation of macroscopic chiral domains in a fluid smectic phase of achiral molecules. Science. 1997;278:1924–1927.

[6] Yu FC, Yu LJ. Mesophases of achiral bent molecules. Chem Mater. 2006;18:5410–5420.

[7] Yu FC, Yu LJ. Mesophases of hockey stick mesogens. Liq Cryst. 2008;35:799–813.

[8] Chakraborty A, Das B, Das MK. New hockey stick compounds with a lateral methyl group showing nematic, synclinic and anticlinic smectic C phase. Liq Cryst. 2011;38:1085–1097.

[9] Chakraborty A, Chakraborty S, Das MK. Effect of hockey-stick-shaped molecules on the critical behavior at the nematic to isotropic and smectic-A to nematic phase transitions in octylcyanobiphenyl. Phys Rev E. 2015;91:032503.

[10] Novotná V, Žurek J, Kozmík V, et al. Novel hockey stick mesogens with the nematic, synclinic and anticlinic smectic C phase sequence. Liq Cryst. 2008;35:1023–1036.

[11] Sathyanarayana P, Radhika S, Sadashiva BK, et al. Structure–property correlation of a hockey stick-shaped compound exhibiting N-SmA-SmC_a phase transitions. Soft Matter. 2012;8:2322–2327.

[12] Horčic M, Kozmík V, Svoboda J, et al. Transformation from a rod-like to a hockey-stick-like and bent-shaped molecule in 3,4′-disubstituted azobenzene-based mesogens. J Mater Chem. 2013;1:7560–7567.

[13] Chakraborty L, Chakraborty N, Sarkar DD, et al. Unusual temperature dependence of smectic layer structure associated with the nematic–smectic C phase transition in a hockey-stick-shaped four-ring compound. J Mater Chem. 2013;1:1562–1566.

[14] Chen D, Wang H, Li M, et al. Chiral random grain boundary phase of achiral hockey-stick liquid crystals. Soft Matter. 2014;10:9105–9109.

[15] Monika M, Prasad V, Nagaveni NG. Hockey stick-shaped azo compounds: effect of linkage groups and their direction of linking on mesomorphic properties. Liq Cryst. 2015;42:1490–1505.

[16] Malkar D, Sadashiva BK, Roy A. Pseudo-polar tilted smectic phases exhibited by bent-core hockey stick shaped molecules. Soft Matter. 2016;12:4960–4966.

[17] Nagaraj M. Dark conglomerate phases of bent-core liquid crystals. Liq Cryst. 2016;43:2244–2253.

[18] Sreenilayam SP, Panov VP, Vij JK, et al. The N_{TB} phase in an achiral asymmetrical bent-core liquid crystal terminated with symmetric alkyl chains. Liq Cryst. 2017;44:244–253.

[19] Alaasar M, Poppe S, Kerzig C, et al. Cluster phases of 4-cyanoresorcinol derived hockey-stick liquid crystals. J Mater Chem C. 2017;5:8454–8468.

[20] Alaasar M, Poppe S, Tschierske C. Cybotactic nematic phases of photoisomerisable hockey-stick liquid crystals. Liq Cryst. 2017;44:729–737.

[21] Begum N, Turlapati S, Debnath S, et al. Achiral unsymmetrical four-ring bent-core liquid crystals with a polar fluoro or chloro end substituent: synthesis and characterisation. Liq Cryst. 2013;40:1105–1115.

[22] Begum N, Kaur S, Mohiuddin G, et al. Structural understanding, photoswitchability, and supergelation of a new class of four ring-based bent-shaped liquid crystal. J Phys Chem B. 2019;123:4443–4451.

[23] Saha SK, Mohiuddin G, Paul MK, et al. Polar switching and cybotactic nematic ordering in 1,3,4-thiadiazole-based short-core hockey stick-shaped fluorescent liquid crystals. ACS Omega. 2019;4:7711–7722.

[24] Dingemans TJ, Murthy NS, Samulski ET. Javelin-, hockey stick-, and boomerang-shaped liquid crystals. structural variations on p-quinquephenyl. J Phys Chem B. 2001;105:8845–8860.

[25] Choi EJ, Park KM, Jeong KU, et al. Synthesis and polar property of new hockey stick-shaped liquid crystals with fluorine substituent. 24th International Liquid Crystal Conference; 2012 Aug 19–24;Mainz, Germany. Abstract 5551_0075.

[26] Belaissaoui A, Cowling SJ, Goodby JW. Spontaneous formation of chiral macrostructures in achiral hockey-stick liquid crystals. Liq Cryst. 2013;40:822–830.

[27] Choi EJ, Park KM, Kim DY, et al. Pseudo-rodlike molecules with hockey-stick-shaped mesogen. Liq Cryst. 2016;43:1597–1605.

[28] Saha SK, Deb J, Sarkar U, et al. Hockey-stick-shaped mesogens based on 1,3,4-thiadiazole: synthesis, mesomorphism, photophysical and DFT studies. Liq Cryst. 2017;44:2203–2221.

[29] Kapuściński S, Wojciechowska A, Urbaniak K, et al. Hockey-stick liquid crystalline 6-oxoverdazyl. Liq Cryst. 2017;44:1093–1110.

[30] Kim JW, Park BW, Yoon TH, et al. Alignment and deformation properties of the third type of hockey stick-shaped molecules in vertical alignment and fringe-field switching modes. Bull Korean Chem Soc. 2018;39:401–404.

[31] Maisch S, Krause AM, Schmidt D, et al. To be or not to be - nematic liquid crystals from shape-persistent V-shaped nematogens with the ‘magic angle’. Liq Cryst. 2018;45(1):136–151.

[32] Wang H, Zhang Q, Chen D, et al. The effect of molecular structure on the chiral random grain boundary phase. Liq Cryst. 2018;45:1234–1241.

[33] Kaur S, Mohiuddin G, Satapathy P, et al. Influence of terminal halogen moieties on the phase structure of short-core achiral hockeystick-shaped mesogens: design, synthesis and structure–property relationship. Mol Syst Des Eng. 2018;3:839–852.

[34] Choi EJ. The past, present, and future of hockey-stick-shaped liquid crystals. Proc of SPIE. 2014;9004:900402-(1–5).

[35] Miyasato K, Abe S, Takezoe H, et al. Direct method with triangular waves for measuring spontaneous polarization in ferroelectric liquid crystals. Jpn J Appl Phys. 1983;22:661–663.

[36] Hegde RS, Kumar J, Prasad V. Achiral bent-core salicylaldimine compounds exhibiting dark conglomerate and B_2 mesophases: effect of linkage groups and lateral substituents. Liq Cryst. 2018;1–17. DOI:10.1080/02678292.2018.1556822

[37] Shanker G, Prehm M, Nagaraj M, et al. Development of polar order in a bent-core liquid crystals with a new sequence of two orthogonal smectic and an adjacent nematic phase. J Mater Chem. 2011;21:18711–18714.